Bioactive Materials 14 (2022) 250–261

Contents lists available at ScienceDirect

Bioactive Materials

journal homepage: www.keaipublishing.com/en/journals/bioactive-materials

Bone targeting antioxidative nano-iron oxide for treating postmenopausal osteoporosis

Liming Zheng [a,b,1], Zaikai Zhuang [a,b,1], Yixuan Li [a,b], Tianshu Shi [a,b], Kai Fu [a,b], Wenjin Yan [a,b], Lei Zhang [a,b], Peng Wang [a,b,c,*], Lan Li [a,b,c,**], Qing Jiang [a,b,c,***]

[a] State Key Laboratory of Pharmaceutical Biotechnology, Division of Sports Medicine and Adult Reconstructive Surgery, Department of Orthopedic Surgery, Nanjing Drum Tower Hospital, The Affiliated Hospital of Nanjing University Medical School, 321 Zhongshan Road, Nanjing, 210008, Jiangsu, PR China
[b] Branch of National Clinical Research Center for Orthopedics, Sports Medicine and Rehabilitation, PR China
[c] Jiangsu Engineering Research Center for 3D Bioprinting, Nanjing, 210008, PR China

ARTICLE INFO

Keywords:
Osteoporosis
Bone targeting
Iron oxide
Antioxidant
Nanomedicine

ABSTRACT

Osteoporosis is the most common degenerative orthopedic disease in the elderly. Recently, the therapeutic methods for osteoporosis have shifted towards the regulation of local immunity in bone tissues, which could provide a suitable environment for the positive regulation of bone metabolism, promoting osteogenic differentiation and inhibiting osteoclast differentiation. Our previous work demonstrated that iron oxide nanoparticles (IONPs) could positively regulate bone metabolism *in vitro*. In this study, we further demonstrated that daily administration of IONPs relieved estrogen deficiency-induced osteoporosis via scavenging reactive oxygen species *in vivo*. Meanwhile, IONPs promoted the osteogenic differentiation of bone marrow mesenchymal stem cells and inhibited the osteoclast differentiation of monocytes from IONPs treated mice. Besides, alendronate, a clinically used anti-osteoporosis bisphosphate, was employed to precisely deliver the IONPs to the bone tissues and played a synergically therapeutic role. Eventually, we verified the bone targeting ability, therapeutic efficiency, and biocompatibility of the novel bone target iron oxides in ovariectomy-induced osteoporotic mice. By applying BTNPs, the OVX-induced osteoporosis was significantly revised in mice models via the positive regulation of bone metabolism.

1. Introduction

Osteoporosis (OP) is a prevalent degenerative orthopedic disease affecting approximately 6.46% of men and 29.13% of women over 50 years old in China [1,2]. The secondary osteoporotic fracture is also a leading cause of disability and death in the elderly [3].

As a common kind of OP occurred in postmenopausal women, postmenopausal osteoporosis (POP) is characterized by increased bone remodeling units, decreased bone formation, and increased bone absorption in each unit [4,5]. Increased bone remodeling units with enhanced bone resorption and damaged bone formation in POP patients may lead to rapid bone loss [4]. Reactive oxygen species (ROS) in the inflammatory extracellular microenvironment are regarded as a critical regulatory factor and a potential target of regulating bone metabolism

Peer review under responsibility of KeAi Communications Co., Ltd.

* Corresponding author. State Key Laboratory of Pharmaceutical Biotechnology, Division of Sports Medicine and Adult Reconstructive Surgery, Department of Orthopedic Surgery, Nanjing Drum Tower Hospital, The Affiliated Hospital of Nanjing University Medical School, 321 Zhongshan Road, Nanjing, 210008, Jiangsu, PR China.

** Corresponding author. State Key Laboratory of Pharmaceutical Biotechnology, Division of Sports Medicine and Adult Reconstructive Surgery, Department of Orthopedic Surgery, Nanjing Drum Tower Hospital, The Affiliated Hospital of Nanjing University Medical School, 321 Zhongshan Road, Nanjing, 210008, Jiangsu, PR China.

*** Corresponding author. State Key Laboratory of Pharmaceutical Biotechnology, Division of Sports Medicine and Adult Reconstructive Surgery, Department of Orthopedic Surgery, Nanjing Drum Tower Hospital, The Affiliated Hospital of Nanjing University Medical School, 321 Zhongshan Road, Nanjing, 210008, Jiangsu, PR China.

E-mail addresses: 15850681759@163.com (P. Wang), lanl17@163.com (L. Li), qingj@nju.edu.cn (Q. Jiang).

[1] These authors contributed equally to this work and should be regarded as first authors.

https://doi.org/10.1016/j.bioactmat.2021.11.012
Received 24 August 2021; Received in revised form 7 November 2021; Accepted 7 November 2021
Available online 24 November 2021

[9,10]. ROS in the inflammatory extracellular microenvironment has a crucial role in inducing uncoupled bone metabolism, enhancing osteoclast differentiation, and inhibiting osteogenic differentiation [11,12]. While conventional treatment for POP is based on the direct regulation of bone metabolism (e.g., bisphosphate, menopause hormone therapy), newly developed therapeutic strategies have focused more on initiative modulation of the local immune environment (to establish a suitable extracellular microenvironment) to keep the bone turnover at an appropriate level [10–12]. The application of antioxidants to scavenge ROS is a novel method independent of the typical therapeutic of bisphosphonates [7,8]. Although bisphosphonates have multiple modes of action in treating POP, it has not been reported as a ROS scavenger yet [13,14]. Antioxidants can block the action of ROS, activate the osteogenic differentiation, mineralization process, and inhibit osteoclasts' formation and activity [13,14,15]. Moreover, a combination of antioxidants and bisphosphonates might be an efficient method for the treatment of POP.

Previous studies suggested that iron oxide nanoparticles (IONPs) could protect mice from ovariectomy (OVX)-induced osteoporosis [17–19]. Furthermore, in our previous work, we discovered that IONPs regulated bone metabolism by scavenging ROS via the Nrf 2-keap1 pathway [20]. Herein, we further demonstrated that IONPs could revise postmenopausal bone loss via scavenging ROS *in vivo*. Following, we used the primary bone marrow mesenchymal stem cells (BMSCs) and monocytes (BMMs) from the IONPs-treated animals and found that the positive regulatory effect of IONPs is dependent on ROS scavenging instead of direct stimulation. Thus, it is feasible to treat POP better by combined application of IONPs with bisphosphonates *in vivo* by the synergistic therapeutic effect.

In present, delivery of nanomaterials to bone tissue remains challenging (low specificity and low clearance), limiting its application in clinical practice [21]. Previous studies demonstrated that phosphate radicals had the ability to be enriched in the bone surface [22–24]. In this study, we designed and synthesized a new bone targeting IONPs (BTNPs) loaded with a Food and Drug Administration (FDA) approved bisphosphonate, alendronate. We found that BTNPs could target to the bone surface and revise postmenopausal bone loss better than the application of IONPs and bisphosphonates. By applying BTNPs, the OVX-induced mice osteoporosis was significantly improved via the positive regulation of bone metabolism (Schematic illustration).

2. Materials and methods

2.1. Materials

All materials were purchased from Sigma Aldrich, and the detailed information was shown in the following section.

2.2. Preparation of BTNPs

IONPs were synthesized using a classic chemical co-precipitation method as previously described [20]. Briefly, 200 mg polyglucose-sorbitol-carboxymethyl ether (PSC) was dissolved in 10 ml ultrapure water of the three-necked flask, and the solution was purified by nitrogen for 5 min to remove oxygen. Then, 30 mg $FeCl_2$ and 60 mg $FeCl_3$ were dissolved in 15 ml ultrapure water. The iron precursor solution was added to the PSC solution. Afterward, 1 g ammonium hydroxide with 28% weight in volume was added into the mixed solution using vigorous mechanical stirring of 800 rpm under 80 °C for 30 min. Next, the solution was collected and dialyzed in membrane tubing (MWCO = 3000) to remove uncoated PSC.

Then, BTNPs were prepared as previously described [25]. 5 mg of IONPs were dispersed in 2.5 ml EDC/NHS solution under vigorous stirring for 12 h at 4 °C to activate the carboxylic acid groups.

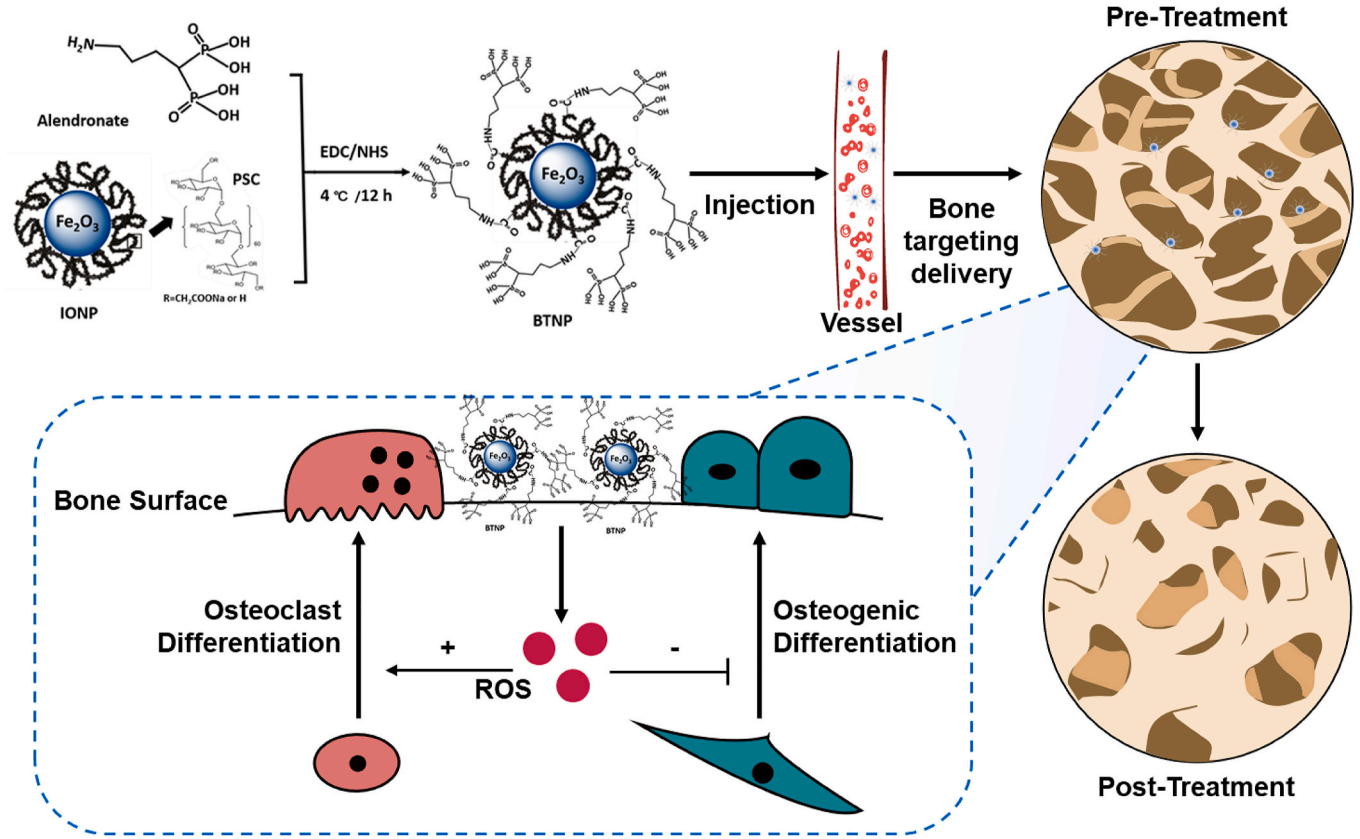

Scheme 1. The BTNPs were prepared by IONPs and alendronate. After the BTNPs were injected intravenously in osteoporotic mice, they were precisely delivered to the bone tissues. By regulating the local level of ROS, the osteoclast and osteogenic differentiation was regulated, and the OVX-induced osteoporosis were treated.

Subsequently, various amount of alendronate was dissolved in 500 μl DMSO. The alendronate solution was added dropwise to the IONPs solution with vigorous mechanical stirring of 1000 rpm for 6 h at 4 °C. Subsequently, the solution was dialyzed in membrane tubing (MWCO = 3000) against 1 × PBS to remove dissociative alendronate. The BTNPs were subsequently stored in the dark at 4 °C. It should be mentioned that both IONPs and BTNPs were sterilized through the use of 0.22-μm membrane filters before further biological assessment.

2.3. Characterization of IONPs and BTNPs

The morphology of IONPs and BTNPs was characterized by transmission electron microscopy (TEM, JEOL 1200EX, Japan). The nanoparticles were dropped on the carbon-coated 400-mesh copper TEM grid and dried completely before TEM observation. The hydrodynamic size and zeta potential of IONPs and BTNPs were obtained by dynamic light scattering (DLS) using a nanoparticle size analyzer (Malvern Zetasizer Nano ZS90, UK). The crystallinity of IONPs and BTNPs was determined by X-ray diffraction (XRD, X'tra, ARL, USA) analysis performed with Cu Kα radiation in the 2θ range of 5°–95° at a scanning rate of 4°/min. Fourier transform infrared spectroscopy (FTIR) was used to identify the presence of amido bond using an infrared spectrometer (VERTEX 80 V, Germany), where the mode was set to the attenuated total reflectance (ATR) and the spectral range was 4000–400 cm^{-1}.

2.4. Animal management

144 female ICR mice (10-weeks-old) were obtained from the Animal Core Facility of Nanjing Medical University. All the animals were housed in a specific pathogen-free environment with a temperature of 22 ± 1 °C, relative humidity of 50 ± 1%, and a light/dark cycle of 12/12 h. All animal studies were performed in compliance with the regulations and guidelines of Drum Tower Hospital institutional animal care and conducted according to the AAALAC and the IACUC guidelines (2019AE01038).

We first evaluated the bone metabolism regulatory effect of IONPs. 48 mice were divided into 4 groups (n = 12 per group), including: Sham group (adipose tissue near ovaries were removed + saline), OVX group (bi-ovaries were removed + saline), IONPs group (Sham + IONPs daily management), and IONPs + OVX group (OVX + IONPs daily management). After the POP models were established for 12 weeks, 100 mg/kg IONPs were intraperitoneally injected twice a week for 8 weeks in IONPs and IONPs + OVX groups. The dosage was determined by our previous work [20]. 24 mice were used for the analysis of therapeutic effect at histological level (n = 6 per group), while the other 24 mice were used for the isolation of primary BMSCs and BMMs (n = 3 per group). Briefly, the femoral and tibia were carefully removed in a sterile environment, and the bone marrow was washed in the determined medium. After being washed by the medium 3 times, the cells were collected by centrifugation at 1500 rpm for 5 min and cultured in a different medium. The detailed information on cell culture was listed in the following section. Cells from each mouse were seeded in three plates for independently repeated experiments.

In the evaluation of the therapeutic effect of BTNPs, 96 mice were used. The mice were divided into 6 groups (n = 16 each group), including: Sham group (adipose tissue near ovaries were removed), OVX group (bi-ovaries were removed), alendronate group (OVX + alendronate), IONP group (OVX + IONPs), LDNP group (OVX + low dosage of BTNPs), and NDNP (OVX + normal dosage of BTNPs). According to previous reports [26,27], monthly intravenous injection (30 mg/60 kg) of alendronate was used for treating osteoporosis. Briefly, 4.55 mg/kg/month alendronate was intravenously injected in the alendronate group according to the equivalent dose calculated by body surface area. The amount of alendronate in the NDNP group was kept the same as the alendronate group. The amount of IONPs in the IONPs group was the same as the NDNP group. In the LDNP group, we injected 1/5 dosage of BTNPs as administrated in the NDNP group. 12 weeks after the ovaries were removed, the drugs were intravenously injected monthly for 8 weeks.

All mice were finally sacrificed, and the femurs, tibias, blood, heart, liver, kidney, spleen, and lung were collected and analyzed *ex vivo*.

2.5. Micro-CT reconstruction and quantitative analysis

For micro-CT analysis, right femurs from mice without soft tissue were dissected and fixed in 4% paraformaldehyde (VivaCT 80, SCANCO Medical AG, Switzerland). The scanner was set at a voltage of 45 kVp, a current of 177 μA, and a voxel size of 15.6 μm. Sagittal images of the distal femur were used for performing the 3D reconstruction and quantitative analysis. The region of interest (ROI) was defined as 624 μm (40 consecutive images) in the proximal position of osteo-epiphysis of the distal femur. Only cancellous bone was used for histological and morphological analysis, and the indexes included BMC (BMD of total volume), BMD (BMD of bone volume), BV/TV (bone volume/total volume) were calculated.

2.6. Paraffin section and histomorphologic measurement

After being fixed with 4% paraformaldehyde for 24 h, femurs were decalcified using a 10% ethylene diamine tetraacetic acid (EDTA) solution. After dehydration and transparency, tissues were embedded in paraffin for the preparation of 5 μm sections. Tartrated Resistant Acid Phosphatase (TRAP) and Masson staining were performed using commercial kits. The same as the ROI chosen in microCT, we selected the cancellous bone in the proximal position of osteo-epiphysis of the distal femur as the ROI for histo-morphologic measurement. The pathological parameters reflecting bone formation (% O. *Pm*) and bone resorption (% Er. *Pm*) were separately marked and calculated in Masson, and TRAP staining results as previously reported [28]. Three high magnification fields of view were randomly selected, and the mean values were used for statistical analysis. Immunofluorescence staining of Runx2, Nox1, Nox4, and SOD1 was performed following a common protocol, and the antibodies were purchased from abcam (the USA).

2.7. Plasma biochemical test and enzyme-linked immunosorbent assay (ELISA) test

Blood was collected from the orbit and stored in an anticoagulant tube with EDTA at 4 °C. Before being used, blood was centrifugated at 3000 rpm for 10 min. The plasma was kept at −80 °C until the ELISA and biochemical detection were performed. Osteoblast-linked indicators, including amino-terminal propeptide of type I procollagen (PINP) and osteocalcin/bone glutamate protein (OT/BGP) and osteoclast-related factor (OSCAR), were detected by ELISA kit (Cusabio, Wuhan, China). The concentration of samples was calculated according to the standard curve calculated. Also, hepatic and renal functions were evaluated by glutamic-pyruvic transaminase (ALT), glutamic oxalacetic transaminase (AST), alkaline phosphatase (ALP), albumin (ALB), and blood urea nitrogen (BUN) in plasma, which was detected by an automatic biochemical analyzer (Rayto, Chemray 240, China) following the manufacturer's instruction manual.

2.8. Preparation of rhodamine B-labeled nanoparticles and in vivo fluorescence imaging (IVIS) evaluation

Rhodamine B-labeled BTNPs were synthesized using a reported method [29]. Briefly, BTNPs powder (200 mg) was dissolved in ultrapure water (1 ml) under the ultrasonic dissolution, followed by the addition of 4 ml dimethyl sulfoxide (DMSO) under vigorous stirring at 50 °C for 30 min. After a drop HCl solution (1 mol/l) was added to the mixed solution to guarantee the carboxylic group activation, carbonyl diimidazole (5 mg), and hydroxybenzotriazole (1 mg) was added under

vigorous stirring at 50 °C for 2 h. After that, ethanediamine (100 μL) was dropwise added to the mixed solution at 50 °C for another 1 h to obtain amino-modified BTNPs. Rhodamine B (5 mg) was dissolved in DMSO (1 ml), followed by the addition of 1-Ethyl-3-(3-dimethylaminopropyl) carbodiimide hydrochloride (EDC, 1 mg), ethanediamine (1, drop) and N-Hydroxysuccinimide (NHS, 1 mg) under vigorous stirring for at least 12 h to obtain rhodamine B–NHS. Finally, the above amino-modified BTNPs solution and rhodamine B–NHS solution were mixed for reaction at 50 °C for another 3 h, followed by the addition of ultrapure water (5 ml) and dialysis in membrane tubing (MWCO = 100 k) against ultrapure water for 2 h to remove dissociative micro-molecules.

Afterward, we used IVIS to evaluate the distribution of the nanoparticles *in vivo*. The mice were intravenously injected with the rhodamine B-labeled nanoparticles, including IONPs and BTNPs. The dosage was kept the same as the experiment performed in the last part. One hour after the nanoparticles were injected, the different organs, including the heart, liver, spleen, lung, and kidney, were taken for IVIS (PerkinElmer). The excitation wavelength was set at 555 nm, while the emission wavelength was set at 580 nm. Those mice treated only with PBS were set as the negative control to adjust the fluorescence images. Six mice in each group were used for the statistical analysis of the fluorescence intensity.

2.9. Evaluation of biocompatibility and drug metabolism

To determine the biocompatibility of BTNPs, we dissected different organs, including the heart, liver, spleen, lung, and kidney, from mice. Tissues were then stained using H&E. An experienced pathologist was invited to evaluate the inflammatory response and structural changes. 24 mice (n = 6 per group) were sacrificed at 24 h post-injection of BTNPs for the bio-distribution study. The major metabolic tissues (heart, liver, spleen, lung, and kidney) were harvested, dried off, and weighed. After been homogenized by concentrated nitric acid, the amount of Fe was measured using ICP-MS (Agilent, 7900). The results were calculated as percentages of injected dose per gram tissue. The final results were expressed as mean ± S.D. (standard deviation).

2.10. Biomechanical analyses

We used a three-point bending test to evaluate the biomechanical characteristic of the right femur. A preload between 1 and 2 N was applied to the midpoint of the diaphysis, and the bone was loaded in bending until failure at a rate of 1 mm/min using an Instron 4465 (Instron, Norwood, MA) with a 1000 N load cell. The modulus of the femurs could be determined from the slope of the obtained stress-strain curve as previous report [30].

2.11. Cell culture

Primary BMSCs and BMMs were separately cultured in stem cell medium (MUBMX-90011, Cyagen) and α-MEM medium supplemented with 30 ng/ml M-CSF. After reaching a cell confluence of 90–100%, cells were cultured in osteogenic (MUBMX-90021, Cyagen) and osteoclast medium (α-MEM medium supplemented with 30 ng/ml M-CSF and 50 ng/ml RANKL) to induce the differentiation. According to the treatment of mice, supplementary agents were added in the medium to enhance the biological effect.

BMSCs were divided into 4 groups and were named the same as the donated mice. BMMs were all taken from the normal mice. The BMMs were divided into 2 groups according to the treatment, including the control and IONPs groups for the osteoclasts' treatment. The supplementary concentration of IONPs was determined as 100 μg/ml according to our previous work.

Raw 264.7 cell line was used for evaluating the ROS level. Briefly, H_2O_2 (100 μM) was used to simulate the inflammatory situation as previously reported [31], and the gradient concentration of IONPs was supplemented. Afterward, the ROS level was evaluated by flow cytometry and fluorescence imaging following a commercial kit (BD Accuri C6, USA).

2.12. Statistical analysis

Data were presented as the style of means ± standard deviation (SD). To calculate the relative expression, a control group was used for standardization. Statistically, a significant difference was determined by *t*-test (2 groups) and one-way ANOVA (Tukey's *post hoc* analysis) when the data met the homogeneity of variance and Gaussian distribution. Otherwise, the non-parametric test was used for the supplement. A significant difference was defined as $p < 0.05$ (*, $p < 0.05$; **, $p < 0.01$; ***, $p < 0.001$; ****, $p < 0.0001$). The graphs were prepared by GraphPad 9.0 software.

3. Results

3.1. IONPs positively regulated bone metabolism in vivo

Firstly, we demonstrated that IONPs could protect mice from OVX-induced osteoporosis. As shown in Fig. 1a, 12 weeks after the ovaries were removed, IONPs were intraperitoneally injected twice a week for 8 weeks. Afterward, the distal femurs were analyzed using a micro-CT (Fig. 1b). The cancellous bone showed a significant decrease post-operatively, while treatment with IONPs protected bone mass from loss. In the quantitative results, the BMC of the sham group was 186.3 ± 37.73 mg HA/ccm, while the value of the IONPs group was not significantly changed (199.7 ± 42.96 mg HA/ccm). In the OVX group, the lower BMC value was 70.18 ± 12.21 mg HA/ccm, indicating the successful establishment of the OP model. With the treatment of IONPs, the BMC significantly increased to 107.5 ± 20.85 mg HA/ccm ($P < 0.01$, Fig. 1c). When it turned to the evaluation of the trabecular parameters, the BV/TV instead of BMD significantly increased, suggesting that the difference of BMC was mainly dependent on affecting bone volume instead of mineralization (Fig. 1c–e).

To further confirm how IONPs affected bone metabolism, we used Masson and TRAP staining to evaluate the situation of bone formation and resorption. As shown in Fig. 1f, the newly formatted osteoid adhered to the bone surface was distinguished and measured to evaluate bone formation. The percentage of the osteoid perimeter (% O. *Pm*) significantly decreased in the OVX group and increased in the IONP group, indicating the reduced bone formation ability in the late-stage POP was enhanced (Fig. 1g). Meanwhile, in the TRAP staining photographs shown in Fig. 1h, the bone resorption surface stained by red increased significantly in OVX group, which could be inhibited by the treatment of IONP. We then calculated the percentage of bone erosion perimeter (% Er. *Pm*) and observed that the increased bone resorption in POP was inhibited by IONPs (Fig. 1i). Next, we used the level of plasma proteins to further evaluate the bone formation (PINP and OT/BPG) and resorption (OSCAR) in Fig. 1j. These indexes showed a similar trend as observed in bone tissues' staining results, demonstrating that IONPs positively regulated bone metabolism in the late-stage OVX mice model.

3.2. IONPs regulated bone metabolism by scavenging ROS

To further explore the potential mechanism of IONPs, we evaluated the level of oxidative stress *in vivo*. The oxidative stress-related proteins, including Nox1, Nox4, and SOD1 were observed increased in POP mice, while the supplementation of IONPs reserved the increase in the immune-fluorescence results (Fig. 2a–d). Afterward, bone marrow mesenchymal stem cells (BMSCs) and monocytes (BMMs) were isolated from mice treated with/without IONPs as described in 3.1. In the process of osteogenic differentiation, BMSCs from OVX mice showed a worse osteogenic ability compared to those from the Sham group ($P < 0.0001$). The treatment of IONPs in the Sham group could not improve the

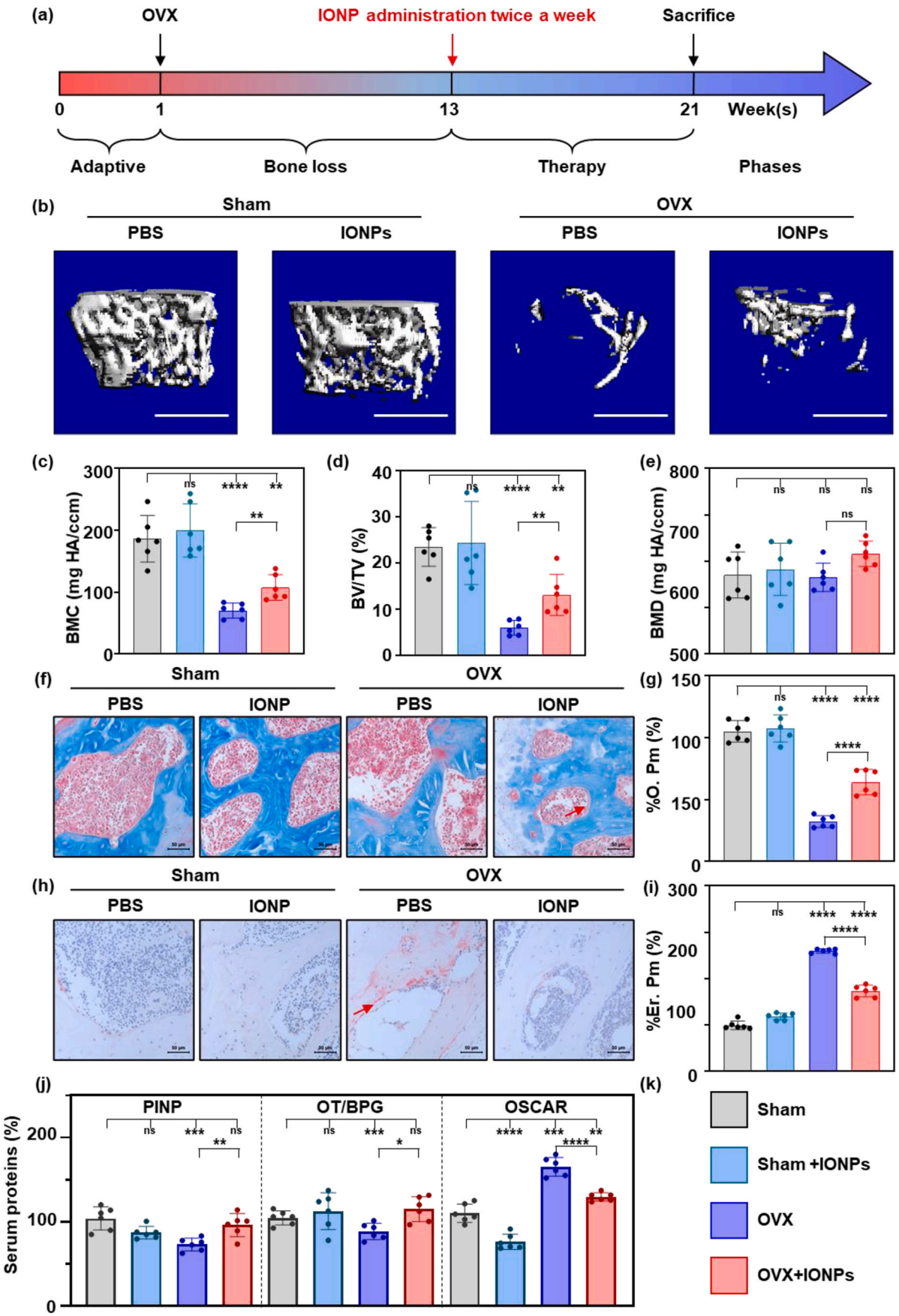

(caption on next page)

Fig. 1. Daily management of IONP positively regulated bone metabolism *in vivo*.
(a)The schematic diagram of the timeline of the *in vivo* test. (b) Micro-CT reconstruction images of the distal femurs of the experimental mice and the quantitative results of BMC (c), BV/TV (d), and BMD (e). (f) Masson staining of bone sections of experimental mice and the quantitative results of % O. *Pm* (g). (h) TRAP staining of bone sections of experimental mice and the quantitative results of % Er. *Pm* (i). (j) The relative plasma proteins expression evaluated by Elisa test, including PINP, OT/BPG, and OSCAR. (k) The legend of all bar charts above. Notes: Scare bars: (b) 1 mm; (f, h) 50 μm. All data are the mean ± s.d. Statistical differences between groups were determined by One-Way ANOVA (Tukey's *post hoc* analysis). **P < 0.01, ***P < 0.001, ****P < 0.0001, ns P > 0.05. n = 6. Red arrow in (f, h) represents the representative osteoid and bone erosion surface.

osteogenic ability. In contrast, the BMSCs from the OVX group differentiated more into bone tissues with the treatment of IONPs (Fig. 2e and f). Following, we evaluated the transcription factor, Runx2, which reflects the translation from BMSCs to osteoblasts (Fig. 2g). In the early stage of osteogenic differentiation (7 days after the osteogenic medium was changed), the translocation of Runx2 into cellular nuclear decreased in those from OVX mice. However, after treatment of IONPs, more Runx2 were seen in the cellular nuclear, suggesting clear BMSCs differentiation into osteoblasts. The ratios of positive and total cells were calculated (Fig. 2h), and the trend is the same as observed in images.

In another aspect, we used BMMs to evaluate the effect of IONPs in osteoclast differentiation. In the OVX mice, the monocytes performed more likely to differentiate into osteoclasts compared to the Sham group, and the process was inhibited by the treatment of IONPs (Fig. 2i). The measurement results of the osteoclasts' area shown in Fig. 2j demonstrated the same trend.

Next, we used a standard monocytes cell line, Raw 264.7, to conduct the antioxidant ability of IONPs. As shown in Fig. 2k, the ROS level significantly increased after being treated with 100 μM H_2O_2, which could be dosage-dependent scavenged by IONPs. In the flow cytometry test results, the ROS level showed the same alter as the fluorescence results (Fig. 2l). In cells treated with H_2O_2, the level of ROS increased to 290.3 ± 28.33% compared with the control group. With the supplementation of 50 and 100 μM IONPs, the level of ROS showed a significant dosage-dependent decrease (176.4 ± 14.64%, and 108.8 ± 7.296%, $P < 0.0001$ compared to 0 μM group).

3.3. Preparation and characterization of BTNPs

To precisely deliver the IONPs to bone tissues, the BTNPs were prepared through amidation between the amino group of alendronates and the carboxyl group of IONPs (Fig. 3a). The amount of alendronate attached on the surface of IONPs was determined by measuring the quantity of alendronate in transudates through centrifugal filtering using ICP-MS for detection of phosphorus amount. About 27 μg alendronate could be coupled with 1 mg IONPs. The FTIR spectra were shown in Fig. 3b. The N–H stretch was observed in 3413 cm^{-1}, confirming the successful conjugation of alendronate [32]. According to the TEM images (Fig. 3c), both IONPs and BTNPs demonstrated dimensional homogeneity and good dispersity, suggesting that the conjugation of alendronate did not affect the morphology of IONPs. The hydrodynamic diameter (Fig. 3d) showed a positive shift from 28.4 nm to 34.9 nm after alendronate conjugation, which is consistent with the previous report [25]. Surprisingly, the polydispersity decreased from 0.15 to 0.067, indicating better mono-dispersity for BTNPs. The Zeta potential was then assessed to reflect the surface potential and stability of nanoparticles. As shown in Fig. 3e, the zeta potential of IONPs and BTNPs was −47.98 mV and −47.75 mV, respectively, indicating that the nanoparticles were negatively charged and stably dispersed in the system. Furthermore, data from XRD patterns (Fig. 3f) showed that all diffraction peaks and relative intensity for IONPs and BTNPs matched well with those of Fe_2O_3, indicating that the alendronate conjugation did not affect the crystallinity of IONPs.

3.4. Evaluation of the bone targeting ability of BTNPs

Afterward, we tested the bone targeting ability of BTNPs *in vivo*. One hour after the agents were intravenously injected into the mice's tail vessel, all tissues, including heart, liver, spleen, lung, and kidney, were taken for the IVIS test. In Fig. 3g, it could be observed that BTNPs were more likely to gather in bone tissues instead of other organs. Also, the femur and lumber were taken for the IVIS evaluation. The fluorescence intensity of BTNPs was significantly higher than in groups injected with PBS and IONPs, suggesting a good bone targeting ability of BTNPs (Fig. 3h–k). Biodistribution data obtained from tissues were determined at 24 h post-injection by ICP-MS measurement. As shown in Fig. 3l, around 0.630 ± 0.020 and 0.294 ± 0.039 μg/mg were left in the liver and spleen for the mice injected with BTNPs, lower than 0.814 ± 0.019 and 0.353 ± 0.022 μg/mg for the one injected with IONPs. A similar tendency was observed for the biodistribution in other major organs. These results indicated that the alendronates could effectively deliver IONPs to the bone tissue, resulting in a decreased tissue uptake dose.

3.5. BTNPs revised OVX-induce bone loss in mice models

After BTNPs were prepared and the bone targeting ability was demonstrated, we evaluated the therapeutic effect *in vivo*. The design of the experiment was shown in Fig. 4a. We firstly used micro-CT to analyze the situation of cancellous bone. As shown in Fig. 4b, the bone mass increased in mice treated with alendronate, low or normal dosage of BTNPs (noted as LDNPs and NDNPs groups). Compared with those in the alendronate group, mice receiving 1/5 dosage of alendronate showed a similar improvement in BMC. In the NDNPs group, the BMC was significantly higher compared with the alendronate group (Fig. 4c). When it turned to BMD and BV/TV, the monthly management of BTNPs enhanced the BMD and BV/TV compared to the OVX group indicating the therapeutic effect of BTNPs (Fig. 4d and e). Moreover, we used a three-point bending experiment to evaluate the mechanical strength of femurs, the modulus of which could be determined from the slope of the obtained stress-strain curve [30]. The application of BTNPs increased the mechanical properties of the bone, suggesting that the therapeutic effect of BTNPs was superior to alendronate (Fig. 4f). Next, we assessed the bone formation and resorption by staining the sections. As shown in Fig. 4g, alendronate and BTNPs improved bone formation activities (Fig. 4h). As for the bone resorption, the erosive bone surface disappeared in the LDNP and NDNP groups (Fig. 4i and j). Also, we evaluated the plasma indexes, including PINP, OT/BGP, and OSCAR, to reflect the alterations in bone metabolism. We discovered that BTNPs positively regulated bone metabolism, enhanced the bone formation, and inhibited the bone resorption (Fig. 4 k-m). Also, the H&E staining sections of the heart, liver, spleen, lung, and kidney (Fig. S1), combined with the plasma indexes shown in Table S1 (ALT, AST, ALP, ALB, and BUN) showed no significant difference, indicating that BTNPs were biosafe for *in vivo* application.

4. Discussion

With the awareness of the pathology of POP has shifted towards the attention of the imbalanced osteoimmune microenvironment, the design philosophy of novel anti-POP drugs has changed to establishing an appropriate environment for positive bone metabolism [6,26]. It has been widely reported that extracellular ROS contributed to the disorder of bone turnover via affecting the extracellular microenvironment, resulting in the occurrence of POP [33]. In our and others' previous works, IONPs were demonstrated linked with the inhibition of inflammation via several pathways and, in turn, regulation of bone metabolism

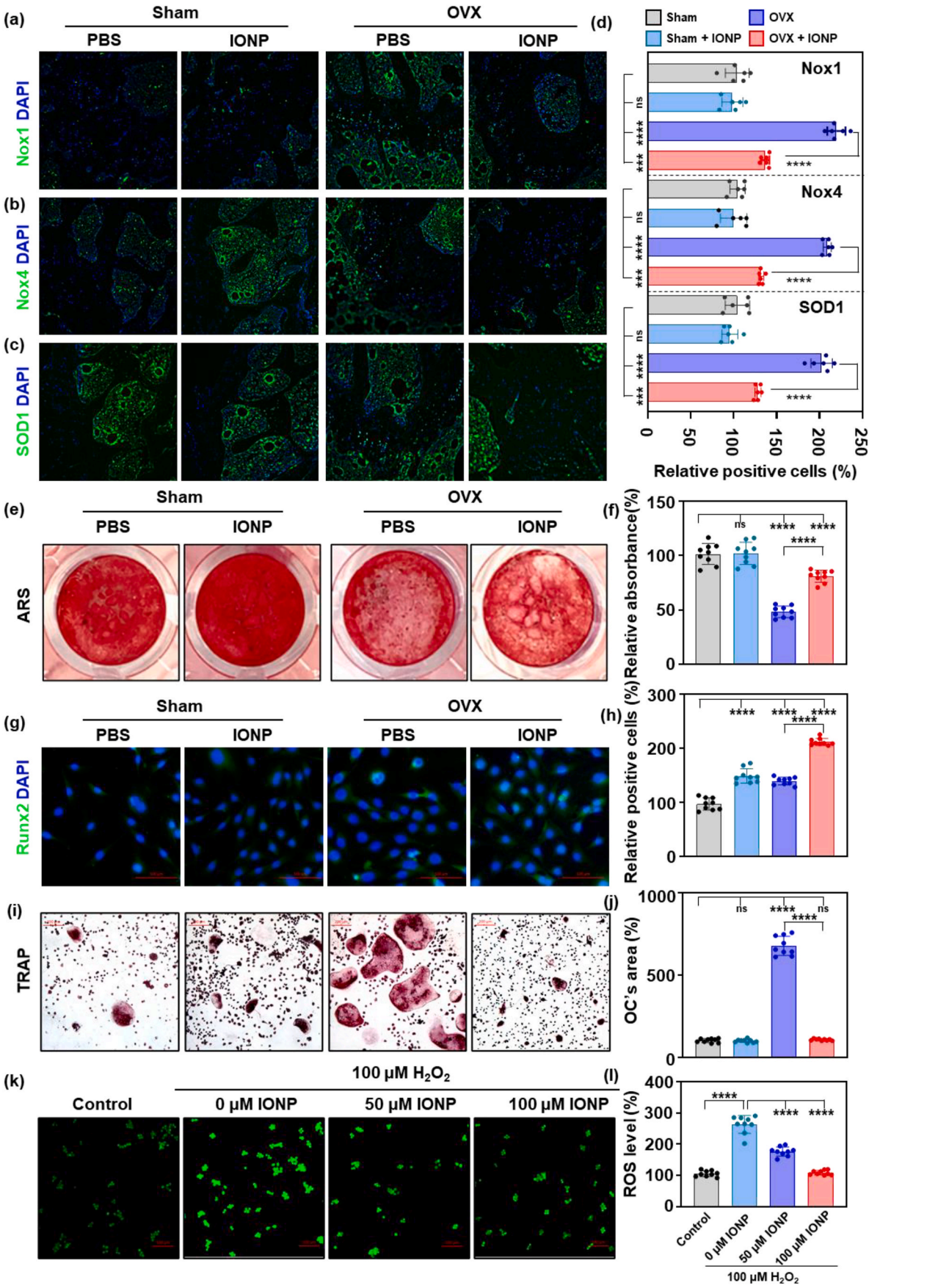

(caption on next page)

Fig. 2. IONPs positively regulated bone metabolism by scavenging ROS.
Immunofluorescence staining images of Nox1 (a), Nox4 (b), and SOD1 (c) in different mice (Blue, DAPI; Green, targeted protein) and the quantitative results (d). (e) ARS staining results of BMSCs from different mice after osteogenic stimulation with/without IONPs for 28 days and the quantitative results (f). (g) Immunofluorescence staining of Runx2 of BMSCs from different mice after osteogenic stimulation with/without IONPs for 7 days (Blue, DAPI; Green, Runx2) and the quantitative results (h). (i) TRAP staining of monocytes from different mice after osteoclastic stimulation with/without IONPs for 7 days and the quantitative results of osteoclasts' area (j). Fluorescence staining images (k) and flow cytometry (l) results of ROS in Raw 264.7 cells. Notes: Scare bars: (a-c, g, k) 100 μm, (i) 200 μm. Sample sizes: (a–d) n = 6. (e–l) n = 9. Statistical differences between groups were determined by One-Way ANOVA (Tukey's *post hoc* analysis). ****P < 0.0001, ns P > 0.05.

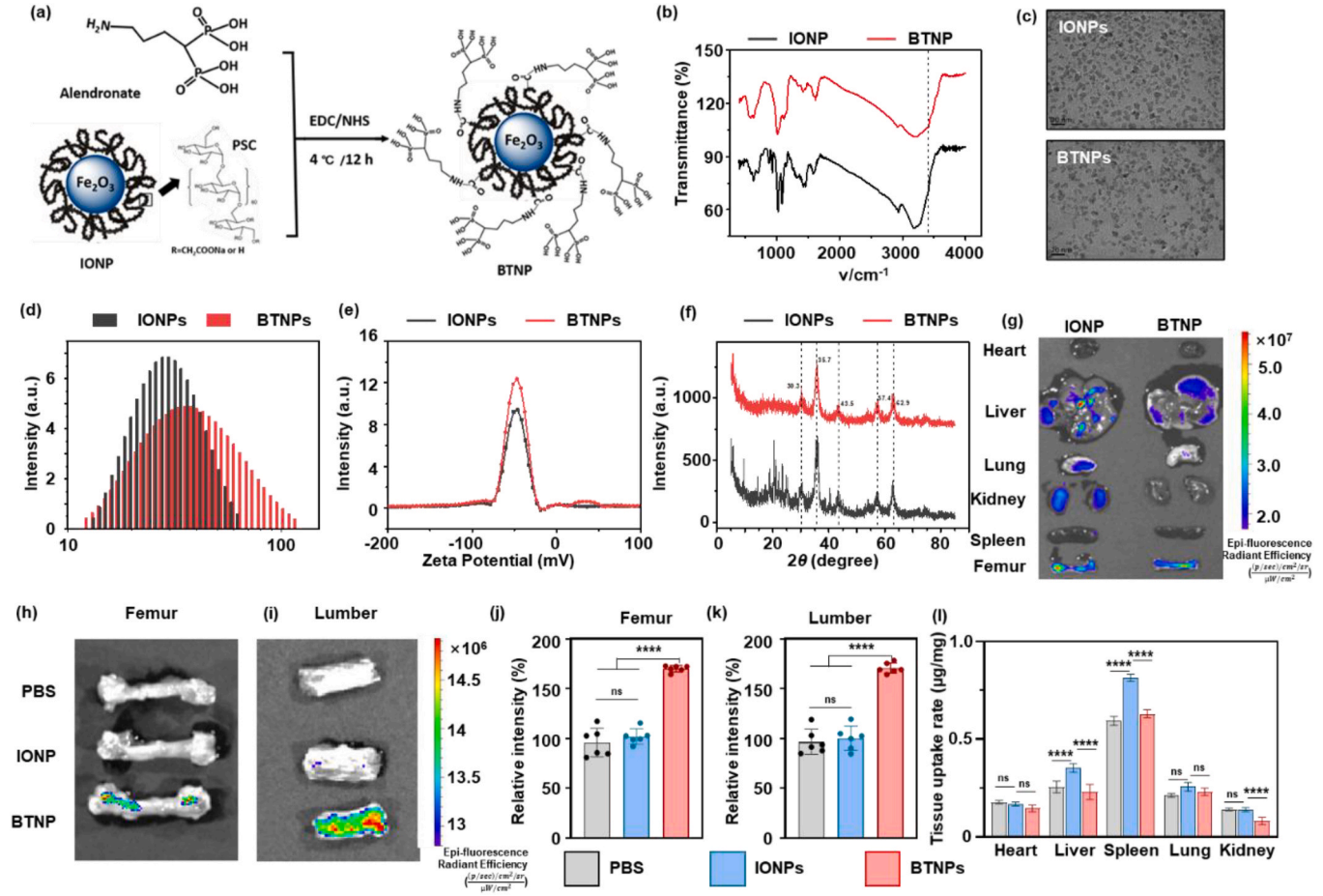

Fig. 3. Preparation and characterization of BTNP.
(a) The schematic illustration of the preparation of BTNP. TEM (b), DLS (c), XRD (d), (e), and Zeta potential (f) results of IONP and BTNP. In vivo fluorescence imaging results of different tissues (g), femur (h), and lumber (i) and quantitative results (j, k). (l) ICP-MS results of tissue uptake of Fe element in different organs including heart, liver, spleen, lung, and kidney. Notes: Scale bar: (c) 20 nm. Sample sizes: (j, k, l) n = 6. Statistical differences between groups were determined by One-Way ANOVA (Tukey's *post hoc* analysis). ****P < 0.0001.

in vitro [20,34,35]. Also, other studies demonstrated that IONPs could positively regulate bone metabolism by adjusting the inflammatory microenvironments *in vitro* [36]. However, there is in lack of *in vivo* experiments to demonstrate the therapeutic effect.

This study is the first to report the feasibility of applying IONPs to treat POP in mice. Our results indicated that long-term management of IONPs is beneficial for bone health by positively regulating bone metabolism via ROS scavenging [37,38]. Our cellular experiments were also performed with primary cells, and the drug administration was performed *in vivo*, which is more closely to the intrinsic situation. Different from the direct action of bisphosphonates on osteogenic and osteoclast differentiation, IONPs regulated bone metabolism by establishing an appropriate environment for drug delivery [16].

In the treatment of POP, systemic application of antioxidants has been accompanied by some unknown side effects [39]. To minimize the side effects and maximize the therapeutic effects, we designed bone-targeting nanoparticles to treat POP in this study. Bisphosphonates and osteoclast targeting peptides are common methods to deliver drugs to bone surfaces [36,40–43]. Considering that bisphosphonates can directly regulate bone metabolism, especially inhibit osteoclast differentiation, independent of the ROS scavenging ability of IONPs [27,44]. We considered that IONPs might have a synergetic effect with bisphosphonates in the aspect of POP treatment. Thus, we chose a common anti-OP drug, alendronate, as the bone targeting moiety [23]. Although the application of bisphosphonates could provide a satisfying therapeutic effect, the side effects caused by treatment, including atypical fracture, nephrotoxicity, and mandibular osteonecrosis, still represent a significant problem [45–47]. Herein, we demonstrated that BTNPs could enhance the therapeutic effect of POP and achieve the same therapeutic effect with just 1/5 dosage of alendronate. As previously reported, a combination of anti-OP drugs and antioxidants, such as Vitamin C/magnesium, magnesium/bisphosphonates, improves the

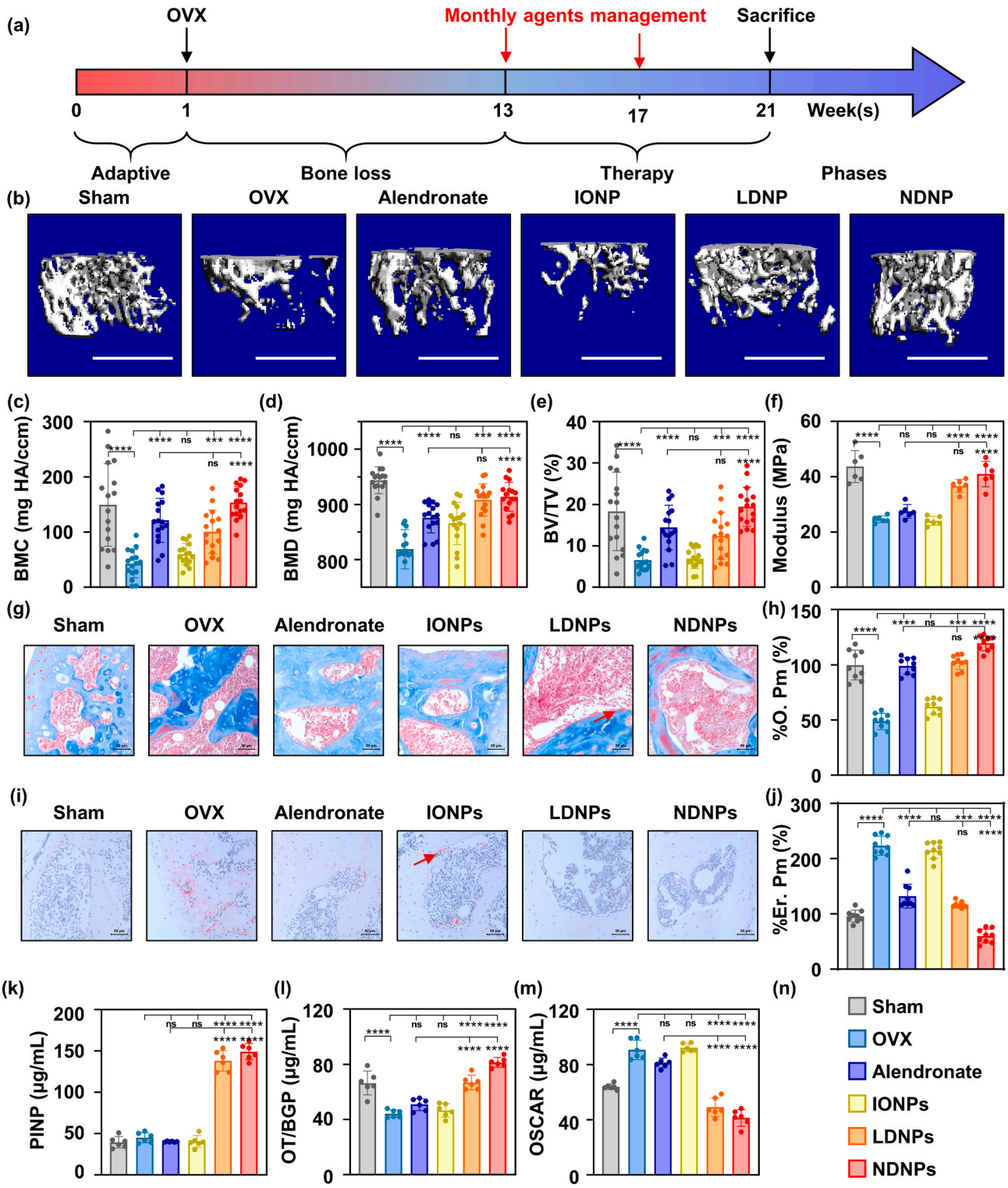

Fig. 4. BTNP protected mice from OVX-induce bone loss *in vivo*.
(a)The schematic diagram of the timeline of the *in vivo* test. (b) Micro-CT reconstruction images of the distal femurs of the experimental mice and the quantitative results of BMC (c), BV/TV (d), and BMD (e). (f) The three point bending test of femurs of the experimental mice. (g) Masson staining of bone sections of experimental mice and the quantitative results of % O. *Pm* (h). (i) TRAP staining of bone sections of experimental mice and the quantitative results of % Er. *Pm* (j). The relative serum proteins expression evaluated by Elisa test, including PINP (k), OT/BPG (l), and OSCAR (m). (n) The legend of all bar charts above. Notes: Scare bars: (b) 1 mm; (g, i) 50 μm. Sample sizes: (a–e) n = 16, (f, k-m) n = 6, (g–j) n = 9. All data are the mean ± s.d. Statistical differences between groups were determined by One-Way ANOVA (Tukey's *post hoc* analysis). **P < 0.01, ***P < 0.001, ****P < 0.0001. Red arrow in (g, i) represents the representative osteoid and bone erosion surface.

drug's therapeutic effect [48–50]. In our work, we chemically coupled IONPs with alendronate and prepared novel nanoparticles, which is convenient for drug management compared to separately injection. Also, we proposed a question that whether the side effect of bisphosphonates could be relieved by the combined application of antioxidants.

In the clinic, severe OP is an intractable clinical problem in need to be urgently solved with the new drugs, which often have some limitations, such as the expensive cost and side effects [51–53]. The BTNPs might be a promising agent to be translated in clinical application. Herein, we demonstrated that BTNPs could enhance the therapeutic effect and achieve the same therapeutic effect with just 1/5 dosage of alendronate. Previously, Ming-Song Lee et al. prepared a similar agent for the treatment of POP [25]. They proved that it is feasible to deliver IONPs to bone tissue by the conjunction of alendronate in IONPs. However, they could only prove that the agent could inhibit the formation of osteoclasts *in vitro*. By delivering the IONPs to the bone resorption area, we confirmed the regulatory effect of IONPs in bone metabolism *in vivo*. Comparison of NDNP group with the alendronate group revealed the increased %O. *Pm* and decreased %Er. *Pm*, which indicated that the IONPs exerted their regulatory effects independent of alendronate. Thus, we believe that the application of antioxidants combined with bisphosphonates is a promising method that could enhance the positive effect on bone metabolism.

As multimodal nanoparticles, BTNPs performed multi-effect *in vivo*. The released IONPs could establish an appropriate environment, while the alendronate acts as the bone targeting moiety and osteoclasts' inhibitor. Also, the bone enrichment property and imaging capability of BTNPs make it possible for future application in specific bone imaging by MRI [54,55,58]. As previously reported, the IONPs could also be used as vehicles for delivering drugs or cells, making the BTNPs a promising nano-sized bone targeting system for future use [56,57]. Collectively, the BTNPs revealed excellent application prospect in clinical use.

5. Conclusions

Our data suggested that IONPs regulated bone metabolism as an antioxidant *in vivo*. In addition, we designed and prepared a novel alendronate-based bone targeting IONPs agent. IONPs and alendronate synergistically exerted therapeutic effects, thus significantly improving the bone mineral density and microarchitecture compared with the same dosage of alendronate. To conclude, we successfully prepared a novel anti-POP agent, which revealed a promising potential to be translated into the clinic.

Author statement

Liming Zheng: Investigation, Conceptualization, Methodology, Formal analysis, Writing - Original Draft, Visualization. Zaikai Zhuang: Investigation, Methodology. Yixuan Li: Investigation, Formal analysis. Tianshu Shi: Investigation, Resources. Kai Fu: Investigation, Resources. Wenjin Yan: Funding acquisition. Lei Zhang: Investigation, Resources, Funding acquisition. Peng Wang: Investigation, Resources, funding acquisition, writing - review & Editing. Lan Li: Investigation, Conceptualization, Methodology, Formal analysis, Writing - Review & Editing. Qing Jiang: Supervision, Writing - Review & Editing, Funding acquisition.

Declaration of competing interest

These authors declared no conflict of interests.

Acknowledgement

This work was supported by Key Program of NSFC (81730067), Major Project of NSFC (81991514), National Science Foundation of China (Grant No 81802135, 82002370), Jiangsu Provincial Key Medical Center Foundation, Jiangsu Provincial Medical Outstanding Talent Foundation, Jiangsu Provincial Medical Youth TalentFoundation, Jiangsu Provincial Key Medical Talent Foundation, the Fundamental Research Funds for the Central Universities (14380493, 14380494), China Postdoctoral Science Foundation (Grant No 2019M661806, Grant No 2020M671456), Natural Science Foundation of Jiangsu Province (Grant No BK20200117, BK20200121), Program of Innovation and Entrepreneurship of Jiangsu Province, Jiangsu postdoctoral research support project (Grant No 2021K059A), Nanjing University Innovation Program for PhD candidates (CXYJ21-62).

Appendix A. Supplementary data

Supplementary data to this article can be found online at https://doi.org/10.1016/j.bioactmat.2021.11.012.

References

[1] Q. Zeng, N. Li, Q. Wang, J. Feng, D. Sun, Q. Zhang, J. Huang, Q. Wen, R. Hu, L. Wang, Y. Ma, X. Fu, S. Dong, X. Cheng, The prevalence of osteoporosis in China, a nationwide, multicenter DXA survey, J. Bone Miner. Res. 34 (2019) 1789–1797. https://doi.org/10.1002/jbmr.3757.

[2] D.M. Black, C.J. Rosen, Postmenopausal osteoporosis, N. Engl. J. Med. 374 (2016) 254–262, https://doi.org/10.1056/NEJMcp1513724.

[3] N.C. Wright, A.C. Looker, K.G. Saag, J.R. Curtis, E.S. Delzell, S. Randall, B. Dawson-Hughes, The recent prevalence of osteoporosis and low bone mass in the United States based on bone mineral density at the femoral neck or lumbar spine, J. Bone Miner. Res. 29 (2014) 2520–2526. https://doi.org/10.1002/jbmr.2269.

[4] R. Eastell, P. Szulc, Use of bone turnover markers in postmenopausal osteoporosis, Lancet Diabetes Endocrinol 5 (2017) 908–923. https://doi.org/10.1016/S2213-8587(17)30184-5.

[5] K. Naylor, R. Eastell, Bone turnover markers: use in osteoporosis, Nat. Rev. Rheumatol. 8 (2012) 379–389, https://doi.org/10.1038/nrrheum.2012.86.

[6] J. Li, C. Deng, W. Liang, F. Kang, Y. Bai, B. Ma, C. Wu, S. Dong, Mn-containing bioceramics inhibit osteoclastogenesis and promote osteoporotic bone regeneration via scavenging ROS, Bioact. Mater. 6 (2021) 3839–3850. https://doi.org/10.1016/j.bioactmat.2021.03.039.

[7] A. Pinna, M. Torki Baghbaderani, V. Vigil Hernández, P. Naruphontjirakul, S. Li, T. McFarlane, D. Hachim, M.M. Stevens, A.E. Porter, J.R. Jones, Nanoceria provides antioxidant and osteogenic properties to mesoporous silica nanoparticles for osteoporosis treatment, Acta Biomater. 122 (2021) 365–376. https://doi.org/10.1016/j.actbio.2020.12.029.

[8] X. Sun, Z. Xie, B. Hu, B. Zhang, Y. Ma, X. Pan, H. Huang, J. Wang, X. Zhao, Z. Jie, P. Shi, Z. Chen, The Nrf 2 activator RTA-408 attenuates osteoclastogenesis by inhibiting STING dependent NF-κb signaling, Redox Biol 28 (2020) 101309. https://doi.org/10.1016/j.redox.2019.101309.

[9] Y. Jiang, W. Luo, B. Wang, X. Wang, P. Gong, Y. Xiong, Resveratrol promotes osteogenesis via activating SIRT1/FoxO 1 pathway in osteoporosis mice, Life Sci. 246 (2020) 117422. https://doi.org/10.1016/j.lfs.2020.117422.

[10] Z. Lin, D. Shen, W. Zhou, Y. Zheng, T. Kong, X. Liu, S. Wu, P.K. Chu, Y. Zhao, J. Wu, K.M.C. Cheung, K.W.K. Yeung, Regulation of extracellular bioactive cations in bone tissue microenvironment induces favorable osteoimmune conditions to accelerate in situ bone regeneration, Bioact. Mater. 6 (2021) 2315–2330. https://doi.org/10.1016/j.bioactmat.2021.01.018.

[11] Z. Chen, J. Yuen, R. Crawford, J. Chang, C. Wu, Y. Xiao, The effect of osteoimmunomodulation on the osteogenic effects of cobalt incorporated β-tricalcium phosphate, Biomaterials 61 (2015) 126–138. https://doi.org/10.1016/j.biomaterials.2015.04.044.

[12] J. Lee, H. Byun, S.K. Madhurakkat Perikamana, S. Lee, H. Shin, Current advances in immunomodulatory biomaterials for bone regeneration, Adv. Healthc. Mater. 8 (2019) 1801106. https://doi.org/10.1002/adhm.201801106.

[13] M.J. Favus, Bisphosphonates for osteoporosis, N. Engl. J. Med. 363 (2010) 2027–2035, https://doi.org/10.1056/NEJMct1004903.

[14] C. Cheng, K. Wentworth, D. Shoback, New frontiers in osteoporosis therapy, Annu. Rev. Med. 71 (2020), https://doi.org/10.1146/annurev-med-052218-020620.

[15] J.E. Compston, M.R. McClung, W.D. Leslie, Osteoporosis, Lancet. 393 (2019) 364–376. https://doi.org/10.1016/S0140-6736(18)32112-3.

[16] M.T. Drake, B.L. Clarke, S. Khosla, Bisphosphonates: mechanism of action and role in clinical practice, Mayo Clin. Proc. 83 (2008) 1032–1045. https://doi.org/10.4065/83.9.1032.

[17] L. Liu, R. Jin, J. Duan, L. Yang, Z. Cai, W. Zhu, Y. Nie, J. He, C. Xia, Q. Gong, B. Song, J.M. Anderson, H. Ai, Bioactive iron oxide nanoparticles suppress osteoclastogenesis and ovariectomy-induced bone loss through regulating the TRAF6-p62-CYLD signaling complex, Acta Biomater. 103 (2020) 281–292. https://doi.org/10.1016/j.actbio.2019.12.022.

[18] M. Li, S. Fu, Z. Cai, D. Li, L. Liu, D. Deng, R. Jin, H. Ai, Dual regulation of osteoclastogenesis and osteogenesis for osteoporosis therapy by iron oxide hydroxyapatite core/shell nanocomposites, Regen. Biomater. 8 (2021), https://doi.org/10.1093/rb/rbab027.

[19] Y. Li, D. Ye, M. Li, M. Ma, N. Gu, Adaptive materials based on iron oxide nanoparticles for bone regeneration, ChemPhysChem 19 (2018) 1965–1979. https://doi.org/10.1002/cphc.201701294.
[20] P. Yu, L. Zheng, P. Wang, S. Chai, Y. Zhang, T. Shi, L. Zhang, R. Peng, C. Huang, B. Guo, Q. Jiang, Development of a novel polysaccharide-based iron oxide nanoparticle to prevent iron accumulation-related osteoporosis by scavenging reactive oxygen species, Int. J. Biol. Macromol. 165 (2020) 1634–1645, https://doi.org/10.1016/j.ijbiomac.2020.10.016.
[21] R. Xu, A. Yallowitz, A. Qin, Z. Wu, D.Y. Shin, J.-M. Kim, S. Debnath, G. Ji, M. P. Bostrom, X. Yang, C. Zhang, H. Dong, P. Kermani, S. Lalani, N. Li, Y. Liu, M. G. Poulos, A. Wach, Y. Zhang, K. Inoue, A. Di Lorenzo, B. Zhao, J.M. Butler, J.-H. Shim, L.H. Glimcher, M.B. Greenblatt, Targeting skeletal endothelium to ameliorate bone loss, Nat. Med. 24 (2018) 823–833, https://doi.org/10.1038/s41591-018-0020-z.
[22] X. Gao, L. Li, X. Cai, Q. Huang, J. Xiao, Y. Cheng, Targeting nanoparticles for diagnosis and therapy of bone tumors: opportunities and challenges, Biomaterials 265 (2021), 120404. https://doi.org/10.1016/j.biomaterials.2020.120404.
[23] J. Hoque, Y.-R. V Shih, Y. Zeng, H. Newman, N. Sangaj, N. Arjunji, S. Varghese, Bone targeting nanocarrier-assisted delivery of adenosine to combat osteoporotic bone loss, Biomaterials 273 (2021), 120819. https://doi.org/10.1016/j.biomaterials.2021.120819.
[24] S. Sun, J. Tao, P.P. Sedghizadeh, P. Cherian, A.F. Junka, E. Sodagar, L. Xing, R. K. Boeckman Jr., V. Srinivasan, Z. Yao, B.F. Boyce, B. Lipe, J.D. Neighbors, R.G. G. Russell, C.E. McKenna, F.H. Ebetino, Bisphosphonates for delivering drugs to bone, 2008–2025, Br. J. Pharmacol. 178 (2021), https://doi.org/10.1111/bph.15251.
[25] M.-S. Lee, C.-M. Su, J.-C. Yeh, P.-R. Wu, T.-Y. Tsai, S.-L. Lou, Synthesis of composite magnetic nanoparticles Fe3O4 with alendronate for osteoporosis treatment, Int. J. Nanomed. 11 (2016) 4583–4594, https://doi.org/10.2147/IJN.S112415.
[26] S.A. Khan, J.A. Kanis, S. Vasikaran, W.F. Kline, B.K. Matuszewski, E. V McCloskey, M.N.C. Beneton, B.J. Gertz, D.G. Sciberras, S.D. Holland, J. Orgee, G.M. Coombes, S.R. Rogers, A.G. Porras, Elimination and biochemical responses to intravenous alendronate in postmenopausal osteoporosis, J. Bone Miner. Res. 12 (1997) 1700–1707. https://doi.org/10.1359/jbmr.1997.12.10.1700.
[27] D.A. Ossipov, Bisphosphonate-modified biomaterials for drug delivery and bone tissue engineering, Expet Opin. Drug Deliv. 12 (2015) 1443–1458, https://doi.org/10.1517/17425247.2015.1021679.
[28] D.W. Dempster, J.E. Compston, M.K. Drezner, F.H. Glorieux, J.A. Kanis, H. Malluche, P.J. Meunier, S.M. Ott, R.R. Recker, A.M. Parfitt, Standardized nomenclature, symbols, and units for bone histomorphometry: a 2012 update of the report of the ASBMR Histomorphometry Nomenclature Committee, J. Bone Miner. Res. 28 (2013) 2–17. https://doi.org/10.1002/jbmr.1805.
[29] H. Cho, D. Alcantara, H. Yuan, R.A. Sheth, H.H. Chen, P. Huang, S.B. Andersson, D. E. Sosnovik, U. Mahmood, L. Josephson, Fluorochrome-functionalized nanoparticles for imaging DNA in biological systems, ACS Nano 7 (2013) 2032–2041, https://doi.org/10.1021/nn305962n.
[30] A. Willems, C. Içli, J.H. Waarsing, S.M.A. Bierma-Zeinstra, D.E. Meuffels, Bone union assessment with computed tomography (CT) and statistical associations with mechanical or histological testing: a systematic review of animal studies, Calcif. Tissue Int. (2021), https://doi.org/10.1007/s00223-021-00904-6.
[31] C.C. Winterbourn, A.J. Kettle, M.B. Hampton, Reactive oxygen species and neutrophil function, Annu. Rev. Biochem. 85 (2016) 765–792, https://doi.org/10.1146/annurev-biochem-060815-014442.
[32] D.L. Pavia, G.M. Lampman, G.S. Kriz, Introduction to Spectroscopy: a Guide for Students of Organic Chemistry, vol. 2009, 1979.
[33] B. Yu, C.-Y. Wang, Osteoporosis: the result of an 'aged' bone microenvironment, Trends Mol. Med. 22 (2016) 641–644. https://doi.org/10.1016/j.molmed.2016.06.002.
[34] I. Merinopoulos, T. Gunawardena, C. Stirrat, D. Cameron, S.C. Eccleshall, M. R. Dweck, D.E. Newby, V.S. Vassiliou, Diagnostic applications of ultrasmall superparamagnetic particles of iron oxide for imaging myocardial and vascular inflammation, JACC Cardiovasc. Imaging 14 (2021) 1249–1264. https://doi.org/10.1016/j.jcmg.2020.06.038.
[35] S.M. Dadfar, K. Roemhild, N.I. Drude, S. von Stillfried, R. Knüchel, F. Kiessling, T. Lammers, Iron oxide nanoparticles: diagnostic, therapeutic and theranostic applications, Adv. Drug Deliv. Rev. 138 (2019) 302–325. https://doi.org/10.1016/j.addr.2019.01.005.
[36] A. Panahifar, M. Mahmoudi, M.R. Doschak, Synthesis and in vitro evaluation of bone-seeking superparamagnetic iron oxide nanoparticles as contrast agents for imaging bone metabolic activity, ACS Appl. Mater. Interfaces 5 (2013) 5219–5226, https://doi.org/10.1021/am4010495.
[37] M. Muñoz, M.E. López-Oliva, C. Rodríguez, M.P. Martínez, J. Sáenz-Medina, A. Sánchez, B. Climent, S. Benedito, A. García-Sacristán, L. Rivera, M. Hernández, D. Prieto, Differential contribution of Nox1, Nox 2 and Nox4 to kidney vascular oxidative stress and endothelial dysfunction in obesity, Redox Biol 28 (2020) 101330. https://doi.org/10.1016/j.redox.2019.101330.
[38] K. Wingler, J.J.R. Hermans, P. Schiffers, A.L. Moens, M. Paul, H. Schmidt, NOX1, 2, 4, 5: counting out oxidative stress, Br. J. Pharmacol. 164 (2011) 866–883. https://doi.org/10.1111/j.1476-5381.2011.01249.x.
[39] G.F. Rushworth, I.L. Megson, Existing and potential therapeutic uses for N-acetylcysteine: the need for conversion to intracellular glutathione for antioxidant benefits, Pharmacol. Ther. 141 (2014) 150–159. https://doi.org/10.1016/j.pharmthera.2013.09.006.
[40] L. Huang, X. Wang, H. Cao, L. Li, D.H.-K. Chow, L. Tian, H. Wu, J. Zhang, N. Wang, L. Zheng, X. Yao, Z. Yang, L. Qin, A bone-targeting delivery system carrying osteogenic phytomolecule icaritin prevents osteoporosis in mice, Biomaterials 182 (2018) 58–71. https://doi.org/10.1016/j.biomaterials.2018.07.046.
[41] X. Wang, B. Guo, Q. Li, J. Peng, Z. Yang, A. Wang, D. Li, Z. Hou, K. Lv, G. Kan, H. Cao, H. Wu, J. Song, X. Pan, Q. Sun, S. Ling, Y. Li, M. Zhu, P. Zhang, S. Peng, X. Xie, T. Tang, A. Hong, Z. Bian, Y. Bai, A. Lu, Y. Li, F. He, G. Zhang, Y. Li, miR-214 targets ATF4 to inhibit bone formation, Nat. Med. 19 (2013) 93–100, https://doi.org/10.1038/nm.3026.
[42] D. Li, J. Liu, B. Guo, C. Liang, L. Dang, C. Lu, X. He, H.Y.-S. Cheung, L. Xu, C. Lu, B. He, B. Liu, A.B. Shaikh, F. Li, L. Wang, Z. Yang, D.W.-T. Au, S. Peng, Z. Zhang, B.-T. Zhang, X. Pan, A. Qian, P. Shang, L. Xiao, B. Jiang, C.K.-C. Wong, J. Xu, Z. Bian, Z. Liang, D. Guo, H. Zhu, W. Tan, A. Lu, G. Zhang, Osteoclast-derived exosomal miR-214-3p inhibits osteoblastic bone formation, Nat. Commun. 7 (2016) 10872, https://doi.org/10.1038/ncomms10872.
[43] Y. Pang, L. Su, Y. Fu, F. Jia, C. Zhang, X. Cao, W. He, X. Kong, J. Xu, J. Zhao, A. Qin, Inhibition of furin by bone targeting superparamagnetic iron oxide nanoparticles alleviated breast cancer bone metastasis, Bioact. Mater. 6 (2021) 712–720. https://doi.org/10.1016/j.bioactmat.2020.09.006.
[44] J.P. Cattalini, A.R. Boccaccini, S. Lucangioli, V. Mouriño, Bisphosphonate-based strategies for bone tissue engineering and orthopedic implants, Tissue Eng. B Rev. 18 (2012) 323–340, https://doi.org/10.1089/ten.teb.2011.0737.
[45] M.A. Perazella, G.S. Markowitz, Bisphosphonate nephrotoxicity, Kidney Int. 74 (2008) 1385–1393. https://doi.org/10.1038/ki.2008.356.
[46] A. Shudo, H. Kishimoto, K. Takaoka, K. Noguchi, Long-term oral bisphosphonates delay healing after tooth extraction: a single institutional prospective study, Osteoporos. Int. 29 (2018) 2315–2321, https://doi.org/10.1007/s00198-018-4621-7.
[47] E.G. Estell, C.J. Rosen, Emerging insights into the comparative effectiveness of anabolic therapies for osteoporosis, Nat. Rev. Endocrinol. 17 (2021) 31–46, https://doi.org/10.1038/s41574-020-00426-5.
[48] L.-Z. Zheng, J.-L. Wang, J.-K. Xu, X.-T. Zhang, B.-Y. Liu, L. Huang, R. Zhang, H.-Y. Zu, X. He, J. Mi, Q.-Q. Pang, X.-L. Wang, Y.-C. Ruan, D.-W. Zhao, L. Qin, Magnesium and vitamin C supplementation attenuates steroid-associated osteonecrosis in a rat model, Biomaterials 238 (2020), 119828. https://doi.org/10.1016/j.biomaterials.2020.119828.
[49] H. Yao, J. Xu, J. Wang, Y. Zhang, N. Zheng, J. Yue, J. Mi, L. Zheng, B. Dai, W. Huang, S. Yung, P. Hu, Y. Ruan, Q. Xue, K. Ho, L. Qin, Combination of magnesium ions and vitamin C alleviates synovitis and osteophyte formation in osteoarthritis of mice, Bioact. Mater. 6 (2021) 1341–1352. https://doi.org/10.1016/j.bioactmat.2020.10.016.
[50] K. Zhang, S. Lin, Q. Feng, C. Dong, Y. Yang, G. Li, L. Bian, Nanocomposite hydrogels stabilized by self-assembled multivalent bisphosphonate-magnesium nanoparticles mediate sustained release of magnesium ion and promote in-situ bone regeneration, Acta Biomater. 64 (2017) 389–400. https://doi.org/10.1016/j.actbio.2017.09.039.
[51] D.L. Kendler, F. Marin, C.A.F. Zerbini, L.A. Russo, S.L. Greenspan, V. Zikan, A. Bagur, J. Malouf-Sierra, P. Lakatos, A. Fahrleitner-Pammer, E. Lespessailles, S. Minisola, J.J. Body, P. Geusens, R. Möricke, P. López-Romero, Effects of teriparatide and risedronate on new fractures in postmenopausal women with severe osteoporosis (VERO): a multicentre, double-blind, double-dummy, randomised controlled trial, Lancet 391 (2018) 230–240. https://doi.org/10.1016/S0140-6736(17)32137-2.
[52] J.-M. Pouillès, A. Gosset, A. Breteau, F.A. Trémollieres, TBS in early postmenopausal women with severe vertebral osteoporosis, Bone 142 (2021) 115698. https://doi.org/10.1016/j.bone.2020.115698.
[53] P.D. Miller, Management of severe osteoporosis, Expet Opin. Pharmacother. 17 (2016) 473–488, https://doi.org/10.1517/14656566.2016.1124856.
[54] S.M. Dadfar, D. Camozzi, M. Darguzyte, K. Roemhild, P. Varvarà, J. Metselaar, S. Banala, M. Straub, N. Güvener, U. Engelmann, I. Slabu, M. Buhl, J. van Leusen, P. Kögerler, B. Hermanns-Sachweh, V. Schulz, F. Kiessling, T. Lammers, Size-isolation of superparamagnetic iron oxide nanoparticles improves MRI, MPI and hyperthermia performance, J. Nanobiotechnol. 18 (2020) 22, https://doi.org/10.1186/s12951-020-0580-1.
[55] H. Wei, O.T. Bruns, M.G. Kaul, E.C. Hansen, M. Barch, A. Wiśniowska, O. Chen, Y. Chen, N. Li, S. Okada, J.M. Cordero, M. Heine, C.T. Farrar, D.M. Montana, G. Adam, H. Ittrich, A. Jasanoff, P. Nielsen, M.G. Bawendi, Exceedingly small iron oxide nanoparticles as positive MRI contrast agents, Proc. Natl. Acad. Sci. Unit. States Am. 114 (2017) 2325, https://doi.org/10.1073/pnas.1620145114. LP – 2330.
[56] D. Ling, N. Lee, T. Hyeon, Chemical synthesis and assembly of uniformly sized iron oxide nanoparticles for medical applications, Acc. Chem. Res. 48 (2015) 1276–1285, https://doi.org/10.1021/acs.accounts.5b00038.
[57] G. Jia, Y. Han, Y. An, Y. Ding, C. He, X. Wang, Q. Tang, NRP-1 targeted and cargo-loaded exosomes facilitate simultaneous imaging and therapy of glioma in vitro and in vivo, Biomaterials 178 (2018) 302–316. https://doi.org/10.1016/j.biomaterials.2018.06.029.
[58] Z.C. Lou, Q.Y. Wang, U.I. Kara, R.S. Mamtani, X.D. Zhou, H.Y. Bian, Z.H. Yang, Y. J. Li, H.L. Lv, S. Adera, X.G. Wang, Biomass-derived carbon heterostructures enable environmentally adaptive wideband electromagnetic wave absorbers, Nano-Micro Lett. (2021), https://doi.org/10.1007/s40820-021-00750-z.

Abbreviations

IONPs: nano-iron oxide;
OVX: ovariectomy; bone targeting nanoparticles
OP: osteoporosis

POP: postmenopausal osteoporosis
ROS: reactive oxygen species
BMSCs: bone marrow mesenchymal stem cells
BMMs: monocytes
FDA: Food and Drug Administration
DMSO: dimethylsulfoxide;
PBS: phosphate buffer saline;
LDNP: low dosage of IONPs
NDNP: normal dosage of IONPs
BMC: bone mineral density of total volume
BMC: bone mineral density of bone volume
BV/TV: bone volume/total volume
EDTA: ethylene diamine tetraacetic acid
TRAP: tartrate-resistant acid phosphatase
PINP: Amino-terminal propeptide of type I procollagen
OSCAR: osteoclast-related factor
ALT: glutamic-pyruvic transaminase
AST: glutamic oxalacetic transaminase
ALP: alkaline phosphatase
BUN: blood urea nitrogen
ALB: albumin
M-CSF: macrophage colony-stimulating factor
RANKL: osteoclast differentiation factor
SD: standard deviation
ANOVA: analysis of variance
micro-CT: micro computerized tomography